nature materials
SUPPLEMENTARY INFORMATION
DOI: 10.1038/NMAT4936

In the format provided by the authors and unedited.

Excitation-wavelength-dependent small polaron trapping of photoexcited carriers in α-Fe_2O_3

Lucas M. Carneiro,[1,4,†] Scott K. Cushing,[1,4,†] Chong Liu,[1,‡] Yude Su[1], Peidong Yang,[1,2,5,6] A. Paul Alivisatos,[1,2,5,6] and Stephen R. Leone*[,1,3,4]

[1]Department of Chemistry, [2]Department of Materials Science and Engineering, and [3]Department of Physics, University of California, Berkeley, California 94720, United States

[4]Chemical Sciences Division and [5]Material Sciences Division, Lawrence Berkeley National Laboratory, Berkeley, California 94720, United States

[6]Kavli Energy NanoScience Institute, Berkeley, California 94720, USA

[‡]Present Address: Department of Chemistry and Chemical Biology, Harvard University, Cambridge, MA 02138, USA

[†]Equal Contribution

Corresponding Author

*E-mail: srl@berkeley.edu.

Charge Transfer Multiplet and Polaron Model of Differential Absorption

a) Charge Transfer State The XUV absorption for the initial optically excited state is predicted using a charge transfer multiplet calculation by CTM4XAS (Reference 29, main paper) with a crystal field splitting of $10Dq$ = 1.45 eV following Reference 26 from the main paper. The optically induced charge transfer can be included by designating the final state to be Fe^{2+}, or by setting the difference between the core hole and Hubbard potential to 5 eV and the hopping parameter for the t_{2g} and e_g band to 2 eV. The latter introduces a ligand-hole on the oxygen site, introducing the optical charge transfer into the CTM4XAS calculation. In order to account for shorter Auger lifetimes at higher energy, the broadening of the x-ray transitions is represented by a Lorentzian with a linearly increasing width from 0.5 eV at 54.5 eV to 2 eV at 56 eV and a Fano asymmetry parameter of 3.5. Instrument resolution is included by a 0.5 eV width Gaussian. The differential absorption is calculated using the difference between the excited state, charge transfer model and the experimentally measured core-hole modified ground state in Figure 1d. For the differential spectrum, a 0.5 eV Lorentzian broadening of the core-hole modified ground state absorption was also found to improve agreement, consistent with an electronic-excited state broadening.

b) Polaron State The polaron state was predicted by convolving the ground state plus core hole XUV absorption with a three-fold energy splitting of the *3p* core level using the values and weighting predicted for Fe^{3+} in $FePO_4$ in Reference 30 of the main paper. The experimental ground state absorption was convolved with a three-fold delta function at energies of 0 eV, 1 eV, and 2.5 eV with weighting of 1/3, 1/2, and 1/6, respectively, which best-fit the data. The differential absorption was calculated by taking the difference between the polaron state absorption and the experimental ground state absorption.

Motivation for Rate Equation Model

Generally, hot electron-phonon equilibration is described in a two-temperature model, where the average occupation statistics of each system are described using their excited state temperature. The temperature is then related to the total energy of the system through the heat capacity, allowing a thermodynamic balance model to be used to describe the thermalization rates. In a two-temperature model, optical excitation first creates a hot electron population. Next, electron-phonon scattering thermalizes the hot electrons by creating a non-thermal optical phonon population. The transfer rate between the two systems is then determined by the electron-phonon scattering time, which must be fit to the data, as well as the relative temperature of each system.

Here, in addition to electron-phonon scattering, an optical phonon and electron can recombine to localize the electron in a small polaron, requiring an additional scattering time to be fit. The exact relationship between the temperature of hot electrons and the amplitude of the charge transfer hybridized state is unknown. Additionally, the optical phonon temperature cannot be directly measured. It is, however, expected that the charge transfer hybridized state amplitude will decrease as the hot electron distribution cools since optical phonon scattering changes the local electronic environment. To simultaneously describe hot carrier thermalization and polaron formation, the two-temperature model can instead be converted into a rate equation with average populations for the hot electrons and optical phonons.

Using the change in the average population instead of a temperature allows a bimolecular recombination term between an electron and optical-phonon to be included to describe small polaron formation. The feedback between hot electron and hot phonon populations, the cooling

rate of hot electrons by scattering with optical phonons, and the possibility of a hot electron combining with an excited phonon to create a polaron can then be described simultaneously. Inclusion of electron and optical phonon scattering with acoustic phonons in the rate equation model does not alter the dynamics because of the low temperatures (<350 K) and short time scales (<3 ps) modeled. Only the polar optical phonons take part in polaron formation, so acoustic phonons would not be expected to directly change the polaron formation rate, only indirectly on longer time scales by influencing the electron or optical phonon population. In this model, small polaron formation is treated statistically, ignoring the spatial nature of the electron and phonon that creates the polaron after excitation.

Derivation of Rate Equation Model for Polaron Formation

The hot electron occupation of a given band *k,* considering all optical phonon absorption and emission processes but ignoring state filling effects, is given by the differential equation:

$$\dot{n_k} = \frac{1}{\tau_{OP}}\left[-(\bar{n}+1)n_k + \bar{n}\, n_{k-q} + (\bar{n}\ +1)n_{k+q} - \bar{n}n_k\right] \qquad (1)$$

where τ_{OP} is the electron-phonon scattering time, $\bar{n}$ is the average occupation of the phonon mode (Maxwell-Boltzmann distribution), and n_i is the electron occupation at the given momentum. The density of states and momentum dependence of τ_{OP} is neglected. The total phonon population for momentum q would then go as

$$\dot{n_q} = -\sum_k \dot{n_{k,q}} \qquad (2)$$

since a phonon is created or destroyed for each emission or absorption process. The transient XUV measurement only gives information about the ensemble-averaged occupation over all energy and momentum, as the transient amplitudes only show to what extent the charge transfer state and polaron state are occupied or not, independent of energy and momentum. To simulate the experimental observables, the sum over all the k and $k\pm q$ connected states can be performed. Assuming the excited electron populations are described by a Boltzmann distribution, this allows Equation 1 to be rewritten as the difference in population between any two states separated by phonon momentum q as

$$\sum\dot{\Delta n_k} = \sum\frac{1}{\tau_{OP}}\left[-(\bar{n}+1)\Delta n_k + \bar{n}\,\Delta n_k\right] = -\sum\frac{\Delta n_k}{\tau_{OP}} \qquad (3)$$

with $\Delta n_k = n_{k+q}\ - n_k$

The sum gives an ensemble averaged change between any two states separated by a phonon of momentum q with an average scattering time of τ_{OP}. To turn Equation 3 into a thermodynamic balance model, the sum can be done over the energy of each state k, giving the ensemble average of the change in energy of the system. This leads to the Two Temperature Model as

$$\frac{dU_e}{dt} = -\frac{C_{V,e}(T_e)\cdot(T_e - T_{OP})}{\tau_{OP}} \qquad (4)$$

$$\frac{dU_{OP}}{dt} = \frac{C_{V,e}(T_e)\cdot(T_e - T_{OP})}{\tau_{OP}} \qquad (5)$$

where $U = C_V(T) \cdot T$ is the energy for each system at constant-volume through the specific heat $C_V(T)$ and temperature T. In equation (4) and (5) the kinetics are summarized in the time dependent change of the average system temperature and dependence on temperature of the specific heat. Here, the relationship between the temperature of the electron, phonon, and polaron and the measured amplitude is unknown. The heat capacity of the polaron is also unknown. Therefore, the sum in equation 3 can instead be taken only over the population, giving the average change in population between any two k states separated by phonon momentum q as

$$\dot{n}_e = -\frac{n_e - n_{OP}}{\tau_{OP}} \quad (6)$$

$$\dot{n}_{OP} = \frac{n_e - n_{OP}}{\tau_{OP}} \quad (7)$$

This allows the polaron to be added in as a bimolecular change in both the electron and hole population. The polaron formation time then describes taking an excited electron at some k and a phonon at some q and removing that population from the ensemble excited state.

$$\dot{n}_e = -\frac{n_e - n_{OP}}{\tau_{OP}} - \frac{n_e \cdot n_{OP}}{\tau_{Pol}} \quad (8)$$

$$\dot{n}_{OP} = \frac{n_e - n_{OP}}{\tau_{OP}} - \frac{n_e \cdot n_{OP}}{\tau_{Pol}} \quad (9)$$

$$\dot{n}_{Pol} = \frac{n_e \cdot n_{OP}}{\tau_{Pol}} \quad (10)$$

Equations 8-10 are fit to the experimental data to obtain the electron-phonon scattering time, the polaron formation time, and two amplitude fit coefficients to relate the predicted population to the change in the experimental differential absorption for the polaron and charge transfer hybridized states. The fitting was done using a robust, multi-start fit method to find the global minimum.

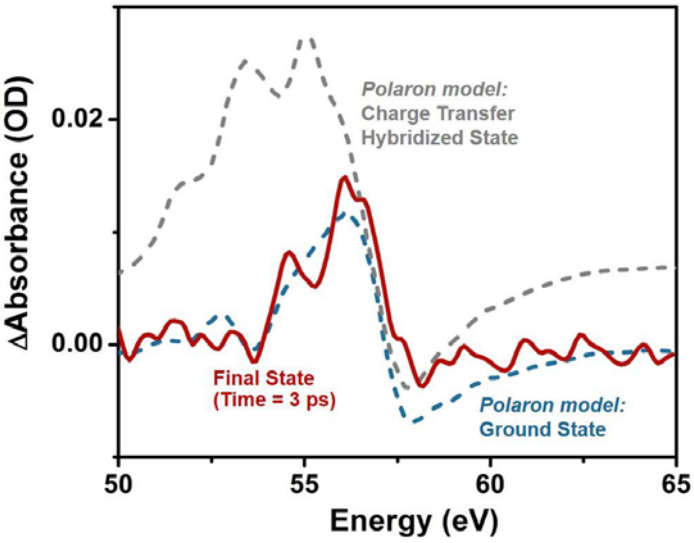

Fig. S1 Differential Absorption Compared to Polaron Models. The differential absorption at *Time = 3 ps* is compared to two polaron models predicted using the splitting of the Fe *3p* core level in either the ground state or the excited, charge transfer hybridized state. The values of the core-level splitting and the assumed amplitude of the polaron state are taken to be the same for both models. Only the polaron model using the ground state can be related to the observed differential absorption. The model using the photoexcited charge transfer hybridized state, consisting of the photoexcited electron and hole, cannot describe the differential absorption. The discrepancy occurs because the charge transfer hybridized state is already red-shifted from the ground state. When the polaron-induced core-level splitting is applied, the spectrum is further redshifted. The change in absorbance below 57 eV is then overestimated compared to polaron splitting of the core-levels in the ground state.

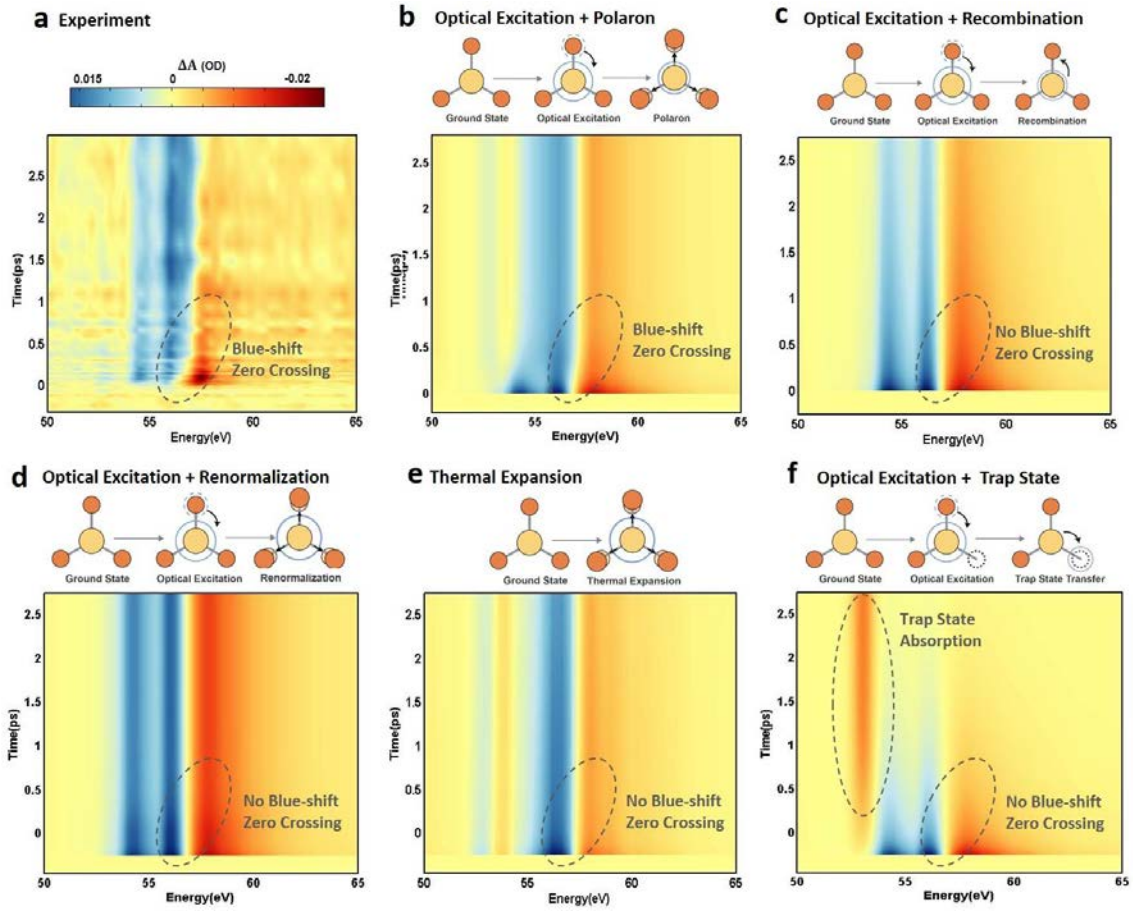

Fig. S2 Possible Recombination Pathways After Optical Excitation. a, The experimental data are compared to the possible recombination pathways after optical excitation. The feature that characterizes the formation of the polaron state is the blue-shift of the zero-crossing around 57 eV, circled for clarity in each plot. **b**, Predicted differential absorption of the charge transfer state and polaron formation. **c,** Charge transfer state and recombination. **d,** Charge transfer state and renormalization representing carrier-carrier, optical phonon, or acoustic phonon based energy shifts. **e,** Thermal lattice expansions. and **f,** Charge transfer state followed by transfer to a defect state. The key regions of absorption are circled for clarity. Only for the polaron formation in **b** does the simulation reproduce the blue-shift of the zero crossing around 57 eV. The charge transfer and polaron state in **b** are simulated as described in the main text. Recombination in **c** is approximated by a three exponential decay of the charge transfer state amplitude with time constants of 100 fs, 1 ps, and 10 ps, matching those commonly inferred from visible light transient absorption literature. Renormalization in **d** is approximated by a 200 fs, 500 meV red-shift of the charge transfer, representing the upper limit of the usually sub 100 meV renormalization caused by carrier-carrier, optical phonon, or acoustic phonon interactions as discussed in the main text. Thermal effects in **e** are approximated by a constant 500 meV red-shift of the ground state, representing lattice expansion. Trap state absorption in **f** is approximated by a 5 percent Gaussian decrease in absorption centered at 53 eV with a width of 500 meV and a 1 ps transfer time from the charge transfer state. A trap state absorption or bleach could occur at the pre-edge of either multiplet peak, however, in neither case is the experimental data in part (**a**) replicated as well as the polaron model of (**b**).

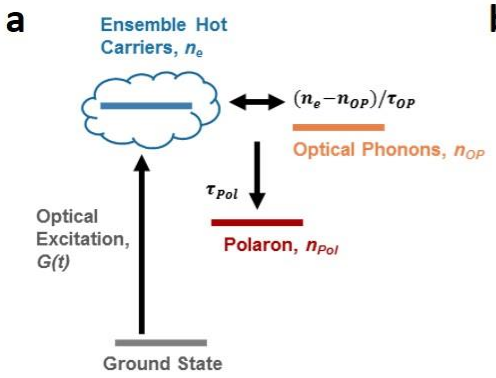

b

$$\frac{dn_e}{dt} = G(t) - \frac{n_e - n_{OP}}{\tau_{OP}} - \frac{n_{OP}n_e}{\tau_{Pol}}$$

$$\frac{dn_{OP}}{dt} = \frac{n_e - n_{OP}}{\tau_{OP}} - \frac{n_{OP}n_e}{\tau_{Pol}}$$

$$\frac{dn_{Pol}}{dt} = \frac{n_{OP}n_e}{\tau_{Pol}}$$

Fig. S3 Polaron Formation Model. a, Following excitation, the optically excited electrons in the charge transfer state thermalize by scattering off of and exciting optical phonons. The optical phonon and electron can then combine to create a polaron. **b,** The rate equation model representing the polaron formation process. Here, *G(t)* represents the excitation source. n_i and τ_i are the population and scattering time for *i=OP* the optical phonons, *i=e* the electrons, and *i=Pol* the polarons. The rate equation model is described in detail at the beginning of the Supplementary Information. The fit is performed using a robust, multi-start algorithm.

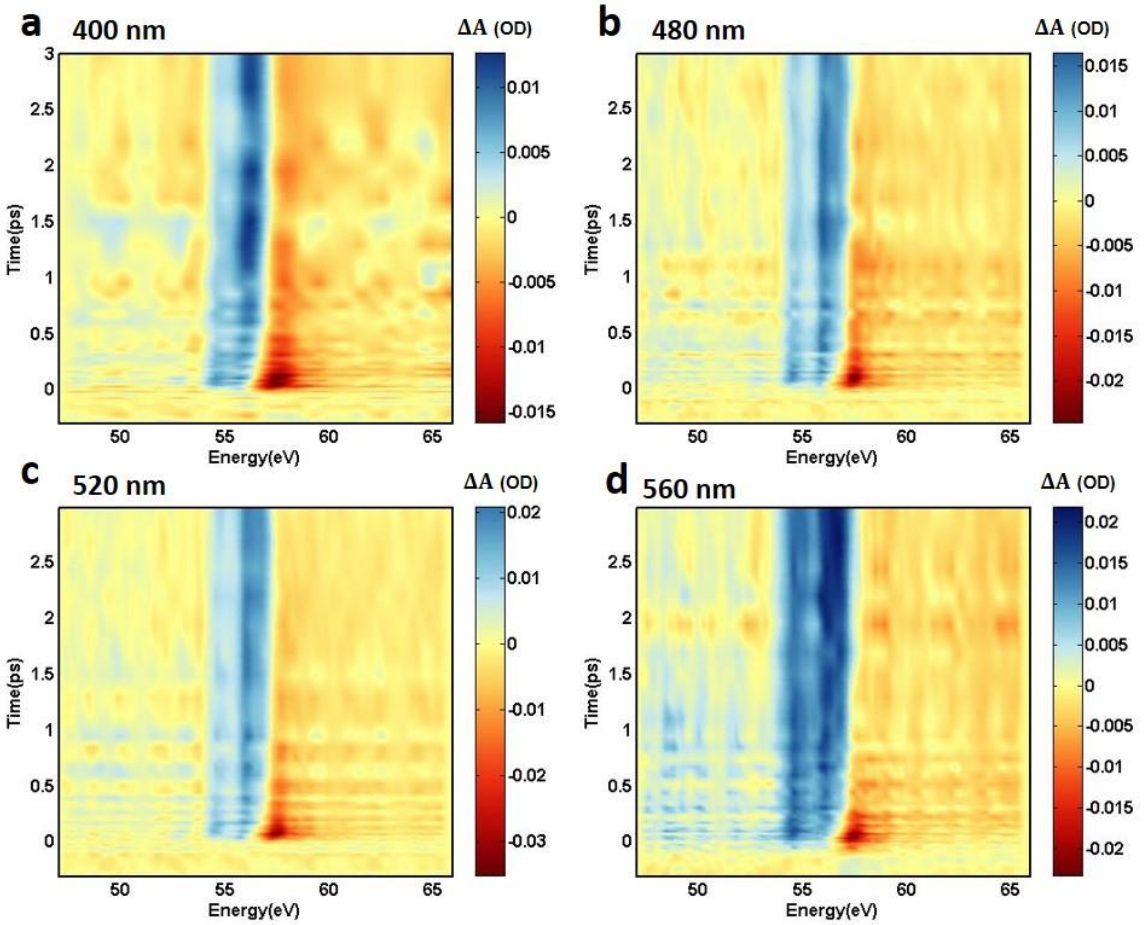

Fig. S4 Experimental Differential Absorption Plots for Several Pump Wavelengths. At each pump wavelength indicated on the figure, the zero crossing point near 56-57 eV between the positive and negative features is seen to blue-shift within ~500 fs. The blue-shift consistently stops within ~2-3 ps.

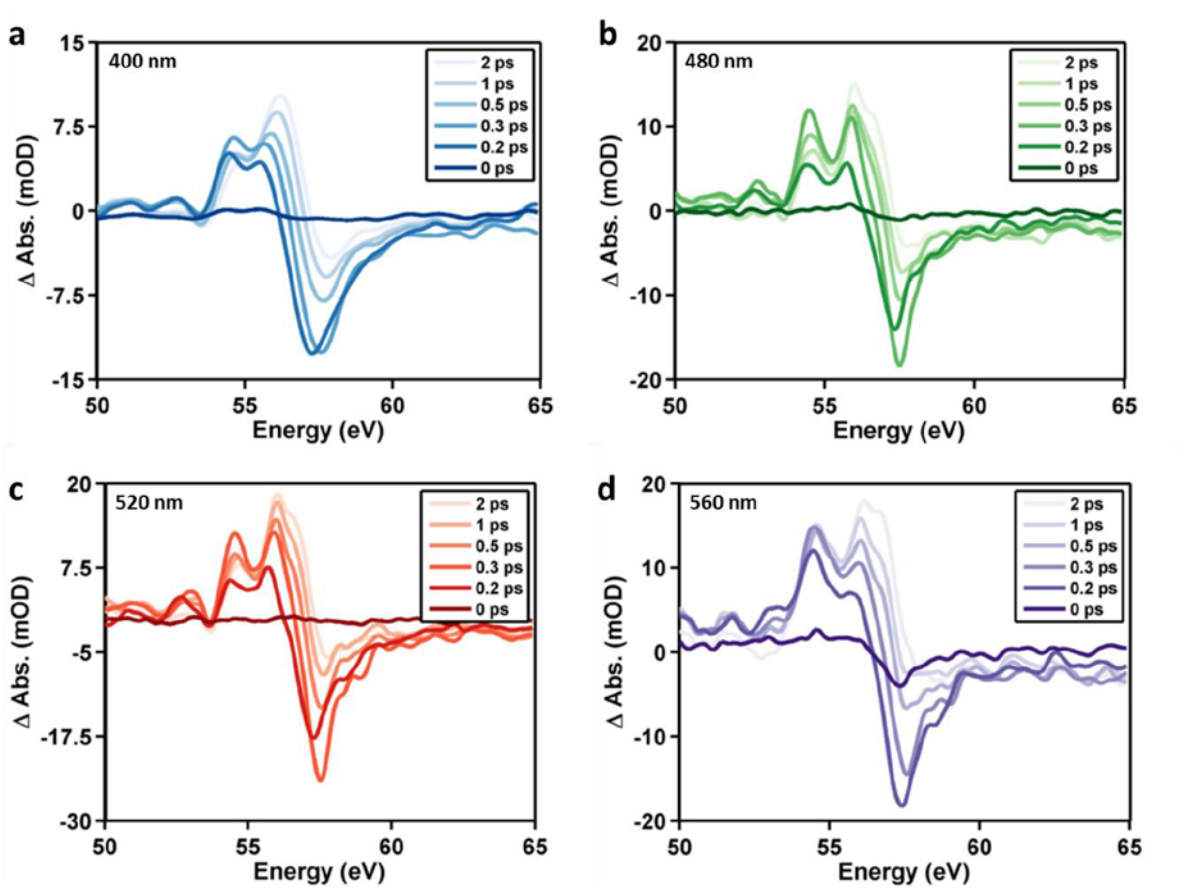

Fig. S5 Differential Absorption Lineouts for Several Pump Wavelengths. Each time point has been averaged over the surrounding 6 time points on a logarithmic scale, isolating the key time periods during relaxation. The zero-crossing between the positive and negative features representing the formation of the polaron is at 56-57 eV. For each pump wavelength, the zero-crossing blue-shifts rapidly within ~500 fs and continues to blue-shift until ~2-3 ps.

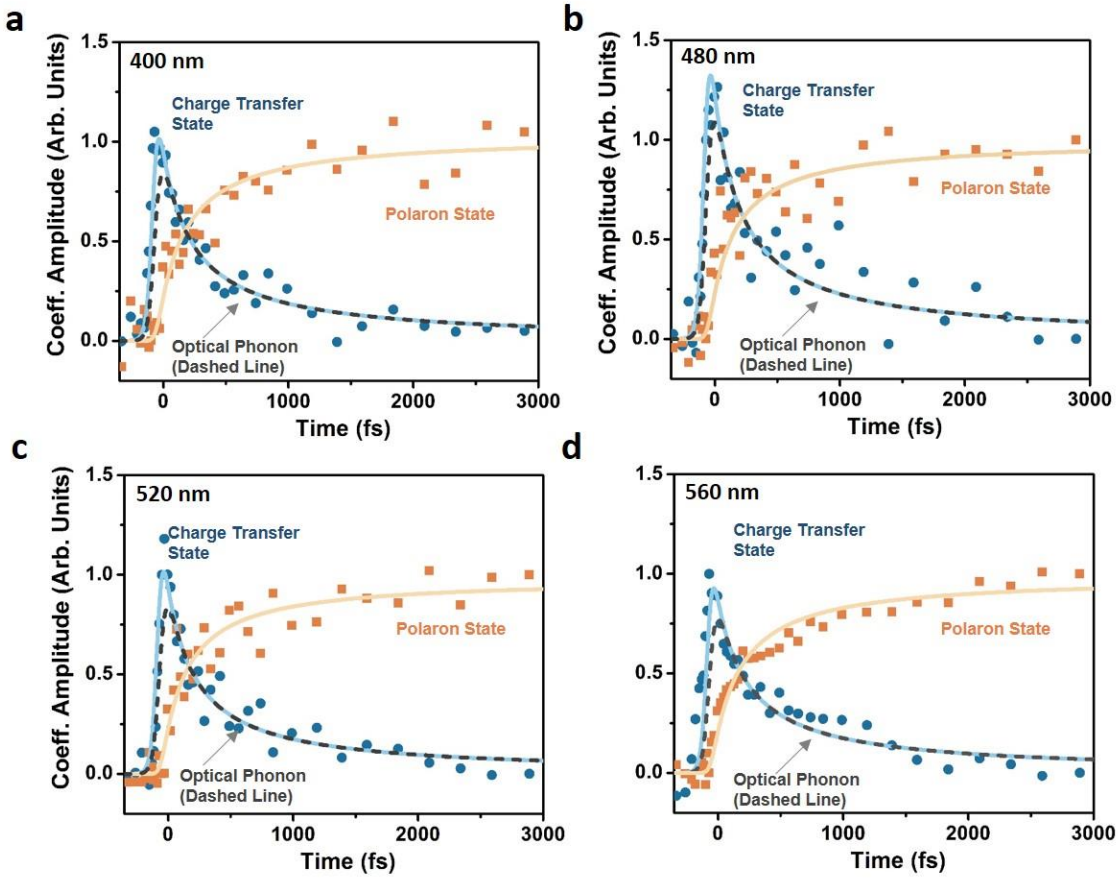

Fig. S6 Polaron Formation Model fit to several Pump Wavelengths. The multivariate regression amplitudes for the charge transfer hybridized and polaron state (circles and squares, respectively) are shown for each pump wavelength indicated on the figure, along with the fit (solid lines) using the rate equation model described in the beginning of the Supporting Information and Figure S2. The scaled phonon population that results from the rate equation model fit is shown for comparison as a dashed grey line. The phonon population is not directly measured in the experiment, so here it is scaled the same as the electron population, which would represent one electron scattering to create one phonon, which then creates one polaron. The deviations from this picture caused by multi-phonon effects are discussed in the text. For each pump wavelength the fitted electron-phonon scattering constant is 30-60 fs, with the insensitivity to electron-phonon scattering time coming from the 50 fs instrument response function of the pump pulse. The fitted polaron formation times are 97±4 fs for 400 nm excitation, 87±5 fs for 480 nm excitation, 88±3 fs for 520 nm excitation, and 100±5 fs for 560 nm excitation.

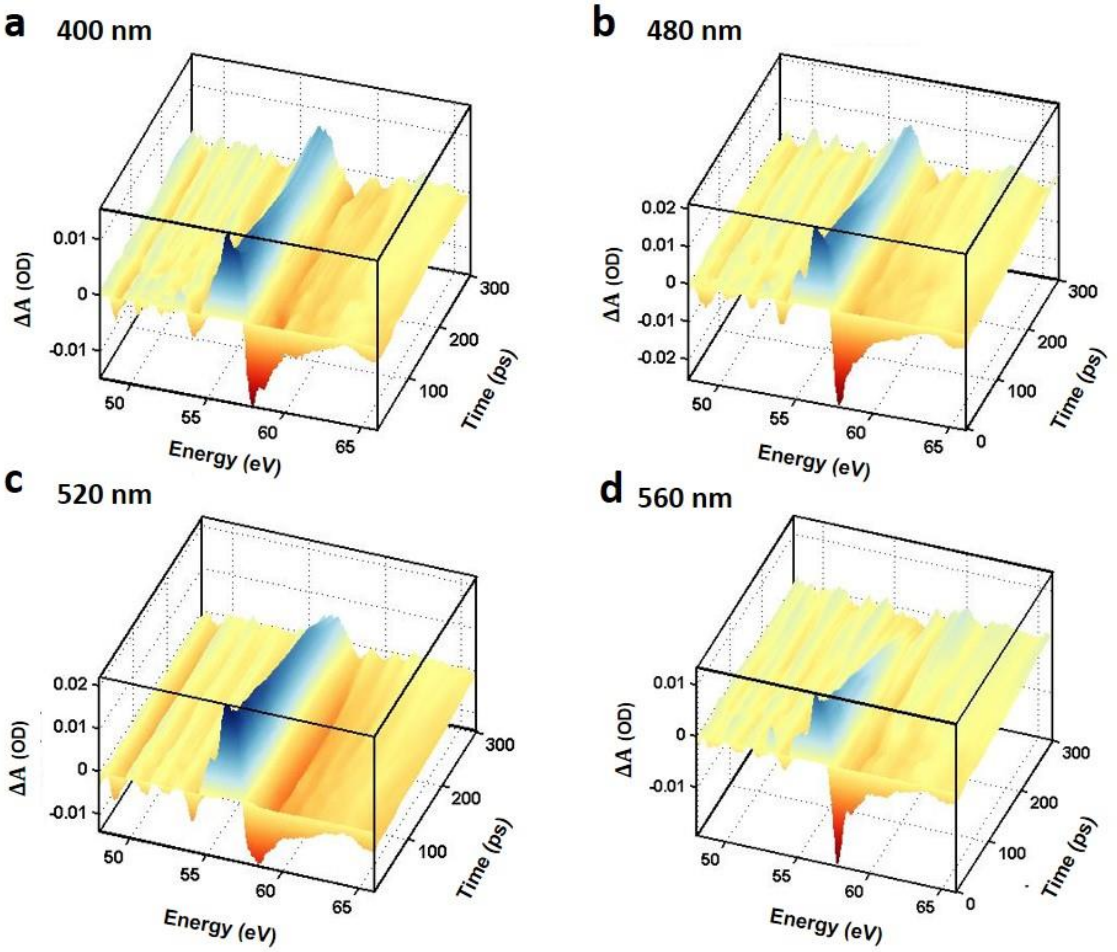

Fig. S7 Experimental Differential Absorption Plots for Long Time Scales at Several Pump Wavelengths. The lifetime of the polaron signal (blue, positive change in absorption) decreases with increasing excitation wavelength. At 560 nm excitation, the polaron signal has decayed to within noise level by ~250 ps.

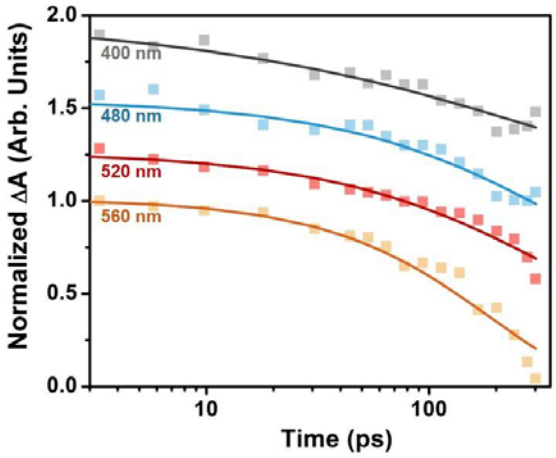

Fig. S8 Stretched-Exponential Fit to Long Time Decay. Squares represent the experimental data, calculated by summing over the polaron peak in Figure S7. Solid lines represent the best fit using the stretched exponential function described in the main text. The excited-state lifetime and the hopping radius increase with increasing excitation energy. The best-fit parameters are tabulated in Table S1. The curves have been offset for clarity.

Table S1 Best fit coefficients for the stretched exponential function, $A \cdot \exp\left(-\left(\frac{t}{\tau}\right)^{\beta}\right)$. Error bars represent the standard error of the fit.

Wavelength (nm)	Amplitude, A	Lifetime, τ (ps)	Stretching Factor, β
400 nm	0.98±0.04	370±50	0.45±0.06
480 nm	0.94±0.03	345±35	0.78±0.1
520 nm	0.96±0.03	344±30	0.76±0.1
560 nm	1.01±0.04	189±15	1±0.15